

Reversible Phasonic Control of a Quantum Phase Transition in a Quasicrystal

Toshihiko Shimasaki¹, Yifei Bai¹, H. Esat Kondakci¹, Peter Dotti¹, Jared E. Pagett¹, Anna R. Dardia¹,
 Max Prichard¹, André Eckardt², and David M. Weld^{1,*}

¹*Department of Physics, University of California, Santa Barbara, California 93106, USA*

²*Technische Universität Berlin, Institut für Theoretische Physik, Hardenbergstraße 36, Berlin 10623, Germany*

(Received 14 December 2023; revised 29 May 2024; accepted 9 July 2024; published 22 August 2024)

Periodic driving can tune the quasistatic properties of quantum matter. A well-known example is the dynamical modification of tunneling by an oscillating electric field. Here we show experimentally that driving the phasonic degree of freedom of a cold-atom quasicrystal can continuously tune the effective quasidisorder strength, reversibly toggling a localization-delocalization quantum phase transition. Measurements agree with fit-parameter-free theoretical predictions, and illuminate a fundamental connection between Aubry-André localization in one dimension and dynamic localization in the associated two-dimensional Harper-Hofstadter model. These results open up new experimental possibilities for dynamical coherent control of quantum phase transitions.

DOI: 10.1103/PhysRevLett.133.083405

Driving can modify the properties of quantum matter [1], tune tunneling [2,3], and control both dynamic [4,5] and Mott localization [6]. While such phenomena have mostly been explored in the context of periodic crystals, richer possibilities exist in non-translationally-symmetric matter. Quasicrystals, which lack both translation symmetry and true disorder, support “phasonic” modes not present in ordinary crystals [7–10] as a consequence of their intrinsic connection to a higher-dimensional superspace [8,11,12], and can exhibit an Anderson-like Aubry-André localization phase transition driven by quasidisorder [13,14]. These properties open up fundamentally new possibilities in the exploration of driven matter.

In this work we demonstrate experimentally and confirm theoretically that driving a phasonic degree of freedom in a cold-atom quasicrystal can tune the effective quasidisorder strength and reversibly control a localization quantum phase transition. As we show, this can be viewed as phasonic Floquet engineering of Aubry-André localization in a 1D quasicrystal, or, equivalently, as tunable dynamic localization by an oscillating electric field in the higher-dimensional quantum Hall system from which the quasicrystal is mapped. These results and complementary perspectives illuminate fundamental connections between apparently different forms of localization, and open up new possibilities for Floquet-engineered matter and dynamical quantum simulation.

The experiments we describe begin by loading an optically trapped Bose-Einstein condensate of $\approx 200\,000$ ^{84}Sr atoms into a bichromatic optical lattice composed of a primary lattice with wavelength $\lambda_P = 1063.9774(23)$ nm

and a secondary lattice with variable depth V_S and wavelength $\lambda_S = 914.4488(17)$ nm (Fig. 1). Ultracold atoms in specialized optical lattices such as this have been shown to provide an ideal platform for the study of quasicrystals [7,15–17]. The experiment is initiated by suddenly extinguishing the confining optical dipole trap after ramping up the bichromatic lattice. This realizes the noninteracting, tight-binding Aubry-André-Harper (AAH) Hamiltonian

$$\hat{H} = -J \sum_{i=1}^L (\hat{b}_i^\dagger \hat{b}_{i+1} + \text{H.c.}) + \Delta \sum_{i=1}^L \cos[2\pi\alpha i + \varphi(t)] \hat{b}_i^\dagger \hat{b}_i, \quad (1)$$

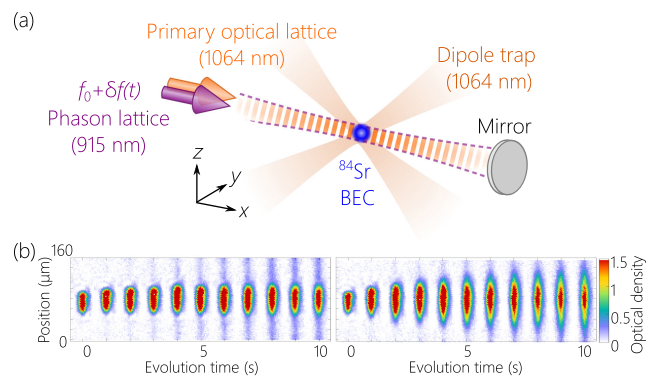


FIG. 1. Experimental schematic and typical data. (a) An optically trapped BEC is loaded into a bichromatic lattice and allowed to evolve. A time-varying phasonic displacement between the two sublattices is controlled by varying the frequency of the secondary lattice laser ($\lambda_S = 915$ nm). (b) Absorption images of the atoms taken after various evolution times in the localized regime (left panel) and delocalized regime (right panel).

*Contact author: weld@ucsb.edu

where J is the tunneling energy which gives rise to a tunneling time $T_J = \hbar/J$, \hat{b}_i^\dagger (\hat{b}_i) is the bosonic creation (annihilation) operator at the i th lattice site, Δ is the secondary lattice depth, $\alpha = \lambda_p/\lambda_S$ is the wavelength ratio of the two lattices, and $\varphi(t)$ is the potentially time-dependent relative phase between the two lattices. This phasonic degree of freedom is controlled by modulating the secondary lattice laser, as described in detail in the Supplemental Material [18], and measured by an interferometer. For $\varphi(t) = 0$ or almost any constant [25], this Hamiltonian exhibits a quantum phase transition at $\Delta = 2J$ between the localized and delocalized phases [13]. When driving the system, in order to avoid the strong interband excitation observed for phasonic driving in [7], we choose modulation frequencies in the optimal frequency window [26] where the modulation is fast compared to the bandwidth but slow compared to the band gap.

We investigate transport in the phasonically driven AAH model by imaging the width σ of the atomic density distribution after some evolution time using *in situ* absorption imaging. Here $\varphi(t) = 2k_S A \sin(\omega t)$, where $k_S = 2\pi/\lambda_S$, A is the phason modulation amplitude, and ω is the phason modulation frequency. A natural question to explore is what happens as the amplitude of phasonic modulation is increased from zero in a regime where the unmodulated system is localized. The first main experimental result of this work is shown in Fig. 2: as the amplitude of phason modulation is increased, the late-time width is greatly enhanced, indicating delocalization, but only at certain modulation amplitudes. The system appears to switch back and forth between localized and delocalized phases as the drive amplitude increases, with late-time width a nonmonotonic function of phason drive amplitude. As a crucial clue to the origin of these delocalization peaks, their peak positions coincide within the resolution of the experiment for three different frequencies, in clear contrast both to dynamic localization [2] and to expected heating behaviors.

To understand this somewhat counterintuitive result, it is helpful to expand the second term in Eq. (1) [7]:

$$\begin{aligned} & \Delta \cos[2\pi\alpha i + 2k_S A \sin(\omega t)] \\ &= \Delta \sum_{n=-\infty}^{\infty} J_n(2k_S A) \cos(2\pi\alpha i - n\omega t), \end{aligned} \quad (2)$$

where J_n are Bessel functions of the first kind. $n \neq 0$ terms, which can lead to multiphason interband transitions [7], can be neglected if the shaking amplitude $2k_S A$ is sufficiently small, and we chose the shaking amplitude A accordingly. More detailed discussion on the effects of the $n \neq 0$ terms is given in Supplemental Material [18]. Keeping only the static $n = 0$ term gives rise to a time-averaged Hamiltonian which is a static AAH Hamiltonian with Δ replaced by a modified effective pseudo-disorder

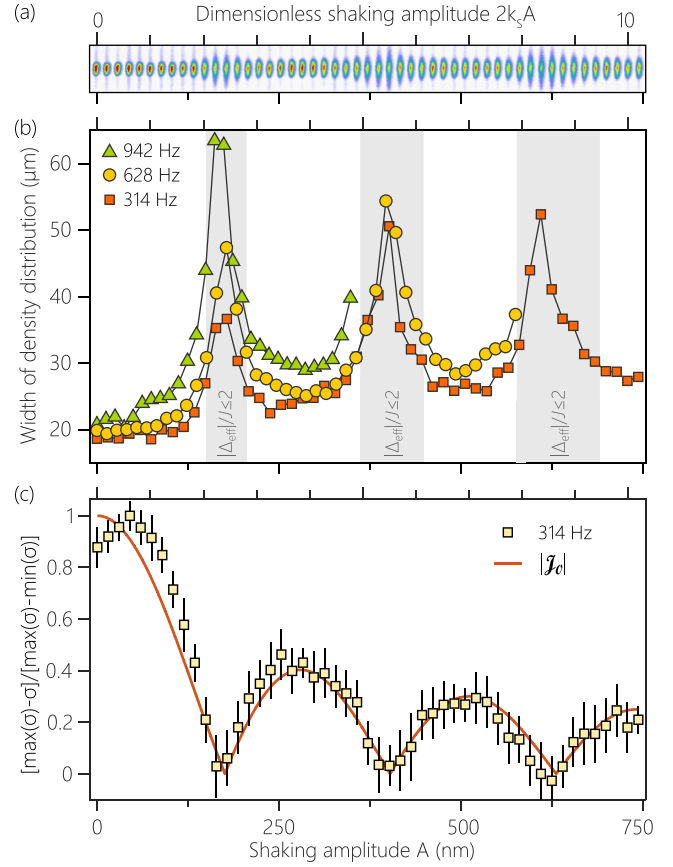


FIG. 2. Phasonic modulation causes dynamic delocalization. (a) Absorption images of the atomic density distribution after 10 s evolution for varying amplitudes of a 314 Hz phason modulation, showing peaks in the late-time width at several drive amplitudes. (b) Width of the atomic density distribution after 10 s evolution versus phason modulation amplitude, for three different driving frequencies. The delocalized regions are observed to be independent of drive frequency. The primary and secondary lattice depths are $10 E_{r,p}$ and $0.5 E_{r,S}$. Here $E_{r,p} = \hbar^2/2m\lambda_p^2$ and $E_{r,S} = \hbar^2/2m\lambda_S^2$ are the recoil energy for the primary and secondary lattice, m is the atomic mass, and \hbar is Planck's constant. Shaded areas show the regime of theoretically predicted delocalization described in the text. (c) Quasi-disorder strength can be inferred from transport. Plot shows a normalized form of the late-time width σ versus phason modulation amplitude, for primary (secondary) lattice depth $8.5 E_{r,p}$ ($0.124 E_{r,S}$), corresponding to the delocalized regime. In this regime the expansion speed is approximately proportional to the quasidisorder strength, so the expected functional form is the absolute value of a Bessel function $|J_0(k_S A)|$, shown here as a solid line with no fit parameters. All of the panels share the same x axis scaling, measured in the dimensionless shaking amplitude $2k_S A$ (panel top) and in the actual shaking amplitude A (panel bottom).

strength $\Delta_{\text{eff}} = \Delta J_0(2k_S A)$. The primary effect of phason modulation is thus to renormalize the effective strength of the incommensurate potential, which becomes a nonmonotonic function of the drive amplitude. If the effective quasidisorder strength falls below $2J$, the system undergoes

a quantum phase transition of the Aubry-André type into the delocalized phase. Figure 2 provides support for this interpretation of the results: the gray shaded areas in Fig. 2(a) indicate the predicted regions of phason drive amplitude where $\Delta_{\text{eff}} < 2J$, and correspond very well to the observed delocalization peaks.

As a more quantitative probe of the Floquet-induced rescaling of quasidisorder, we measured transport starting in a delocalized regime with a lower secondary lattice depth. In this regime, the speed of the ballistic expansion is approximately proportional to the dimensionless distance from the localization phase transition $2 - \Delta_{\text{eff}}/J$, a feature we have confirmed numerically [18]. For this reason, a plot of the appropriately normalized late-time width of the density distribution as a function of $k_S A$ should take on the exact form of a Bessel function, with an absolute value since such transport measurements do not distinguish positive from negative quasidisorder. Figure 2(c) shows just such a plot of normalized late-time widths; the measured data are overall in excellent agreement with a $|J_0|$ Bessel function without any fit parameters. The slight theory-experiment disagreement at low shaking amplitudes is not completely understood.

An intriguing connection emerges when these results are interpreted in terms of the higher-dimensional superspace associated with any quasiperiodic system. The 1D AAH model can be obtained by dimensional reduction from the 2D anisotropic Harper-Hofstadter model with lattice spacing a describing a 2D electron gas in a high magnetic field [11,27,28] [18], in a gauge where the vector potential $\mathbf{A} = [0, 2\pi\alpha x/a + \varphi(t), 0]$ and zero scalar potential:

$$\hat{H}_{2\text{D,HH}} = \sum_{x,y} -J\hat{c}_{x+1,y}^\dagger \hat{c}_{x,y} + \sum_{x,y} \frac{\Delta}{2} e^{-i[2\pi\alpha x/a + \varphi(t)]} \hat{c}_{x,y+1}^\dagger \hat{c}_{x,y} + \text{H.c.} \quad (3)$$

Here the quasidisorder strength Δ becomes the tunneling strength along the extra dimension in the superspace, the incommensurate ratio α describes the magnetic flux per plaquette, and the time derivative $-\partial_t \varphi(t)$ of the phasonic parameter appears as an applied electric field along the extra dimension. The sinusoidal modulation $\varphi(t) = 2k_s A \sin \omega t$ thus corresponds to a driven Harper-Hofstadter model strongly irradiated by light linearly polarized along the extra dimension in the superspace. In particular, the rescaling of the quasidisorder Δ which we observe in the 1D model corresponds to a rescaling of tunneling along that dimension. This provides a complementary picture of the destruction of localization we observe, which in the higher-dimensional space appears as coherent destruction of tunneling along the extra dimension [29], causing the 2D square lattice to decompose into a set of decoupled one-dimensional chains that cannot support localized modes. Besides providing an alternative

perspective, the superspace picture can also be used [30] to design modulation protocols which perfectly destroy localization in a generic bounded quasiperiodic system, by connecting to the concept of exact dynamic localization [31,32]. This higher-dimensional mapping extends the applicability of our results to other quasiperiodic systems [33,34] and also implies an interpretation of our results as the observation of dynamic localization in a strongly driven Harper-Hofstadter model.

Because dynamic localization is coherent [6], phasonic modulation can be used as a tool to reversibly and coherently control transport. To experimentally test this possibility we performed transport measurements for several different driving sequences during which phason modulation is turned on and off at different times during the course of an experiment. Figure 3 shows the results of these experiments, compared to evolution in a static primary lattice and in a static bichromatic lattice. In a bichromatic lattice subjected to continuous phason modulation, the system evolves in a delocalized way, with width growing nearly as fast as when the secondary lattice was entirely absent. This further supports the notion that the quasiperiodic potential effectively vanishes at these resonant amplitudes. For a modulation protocol where phasonic driving is present only for the first 0.5 s of the evolution, the width grows rapidly in accordance with the delocalized expectation until the drive ceases, at which point the system localizes and the width becomes static. This observation indicates that the drive-induced delocalization is not due to significant heating or interband excitation, but rather represents coherent control of the localization properties. Anderson-type localization requires wave packet coherence, and dephasing across lattice sites generally leads to delocalization as the coherence is destroyed [35,36]; the fact that the atoms relocalize when the phasonic modulation is turned off indicates that coherence is maintained throughout the experiment. Finally, if phasonic modulation is applied only during the middle 0.5 s of the sequence, the width evolves in a localized way before the drive, then grows rapidly during the delocalized segment, then ceases to grow when the drive is removed. The last two coherent control protocols result in an identical width at the end of the experiment despite their different modulation histories. Together these results clearly demonstrate that phasonic driving can reversibly and coherently control a localization quantum phase transition.

A new direction opened up by this capability is investigation of the interplay between dynamic localization (induced by a time-varying electric field) and Aubry-André localization (induced by quasidisorder) [37,38]. Using the capabilities demonstrated above, both these types of localization can now be Floquet tuned. In a final set of experiments we investigated this interplay, using phase modulation of just the primary lattice. For this experiment, we modified the setup of Fig. 1 so that the

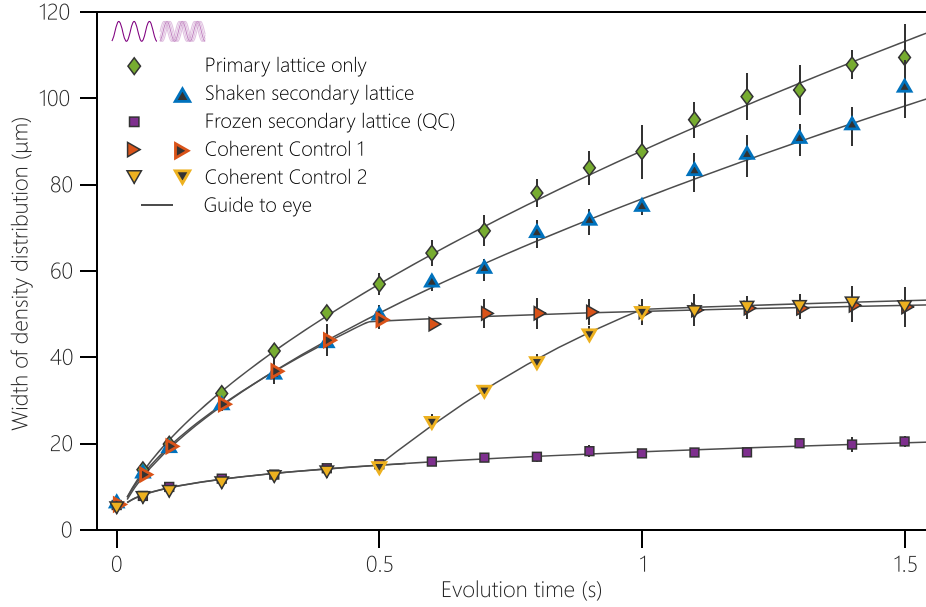


FIG. 3. Reversible coherent control of localization. Symbols show measured late-time width of the density distribution versus hold time for five different experimental protocols: no secondary lattice (diamonds), continuous phasonic driving of secondary lattice (upward triangles), phasonic driving for the first 500 ms (rightward triangles), phasonic driving only between 500 and 1000 ms (downward triangles), and no driving of the secondary lattice (squares). For all protocols the primary lattice depth is $6 E_{r,p}$, and for all but the first plot the secondary lattice depth is $0.5 E_{r,s}$. At these values in the absence of driving the system is Aubry-André localized. Note especially that width evolution under the second “coherent control” protocol shows evidence of localization for times less than 0.5 s and greater than 1 s, and evidence of delocalization between those times, indicating reversible coherent control. Shaking frequency is 628 Hz and phason amplitude is $2k_S A \approx 5.52$, near the second Bessel zero.

primary lattice could be phase modulated using paired acousto-optic modulators controlling the two beams comprising the lattice. In the co-moving frame of the shaken primary lattice, the atoms then experience both a phasonic modulation of the secondary lattice, which tunes Aubry-André localization, and an alternating inertial force, which tunes the tunneling matrix element and drives dynamic localization. In the higher-dimensional picture described above, this corresponds to irradiation with elliptically polarized light.

Figure 4 shows the results of these experiments. The top panel shows the calculated effective tunneling matrix element as a function of the shaking amplitude $K_0 = \pi \Delta \nu_{\max} / 4 f_{r,p}$, where $\Delta \nu_{\max}$ is the frequency modulation amplitude for the modulated primary lattice beam and $f_{r,p} = E_{r,p} / 2\pi \hbar$ as defined in [2,39]. The alternating inertial force rescales tunneling, controlling the overall expansion dynamics, and leading to dynamic localization at $K_0 \approx 2.4$. However, since the modulation of the primary lattice also gives rise to phasonic driving, Aubry-André delocalization can compete with this overall localizing trend, as modulation of the secondary lattice in the comoving frame rescales the secondary lattice depth by the factor $J_0(2k_S A)$. Since the phasonic modulation amplitude A is related to K_0 by $A = (\lambda_p f_r / \pi^2 f) K_0$, the same K_0 can correspond to different shaking amplitudes of the secondary lattice depending on the frequency of the phase

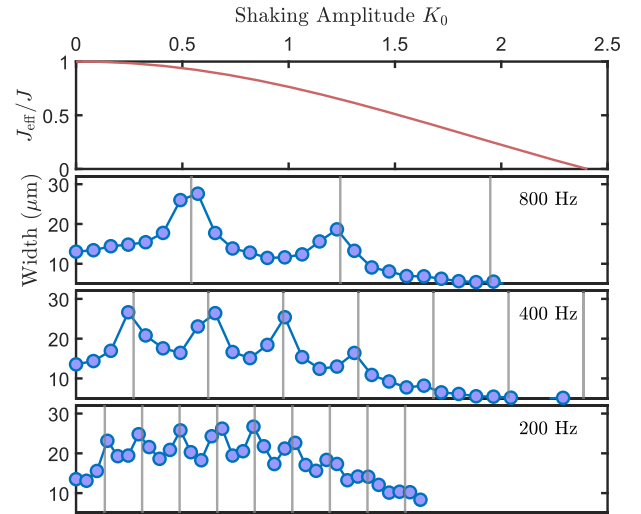


FIG. 4. Interplay between dynamic localization and Aubry-André localization revealed by phase modulation of only the primary lattice. Top panel shows calculated effective tunneling strength as a function of modulation amplitude K_0 . Lower panels show measured width of the density distribution after 1 s expansion in a bichromatic lattice with only the primary lattice shaken, for various modulation frequencies as indicated. Gray lines indicate theoretically expected values of zero effective quasidisorder, as described in the text.

modulation. The bottom panels of Fig. 4 show the late-time density distribution width after expansion in a bichromatic lattice with the primary lattice shaken at different frequencies f . While all of the panels in Fig. 4 share the same K_0 axis, A depends on the drive frequency. At each drive frequency, we observe an array of delocalizing peaks superimposed upon the overall trend towards dynamic localization as K_0 increases. The arrangement of delocalized peaks varies with the drive frequency, and the position of all observed delocalized peaks matches well to zeros of $J_0(2k_S A)$, indicated by gray lines in each panel. This close match to fit-parameter-free theory provides strong support for the interpretation of these delocalized peaks as being due to phasonic rescaling of the secondary lattice depth to zero in the comoving frame.

These results highlight the rich interplay between two distinct forms of localization, and open up additional possibilities. While in this work both phenomena were tuned with a single lattice modulation, a full exploration of the phase diagram of matter subjected to both dynamic localization and Aubry-André localization, as envisioned in [40], would require separately controlling dynamic localization and the rescaling of the secondary lattice.

In summary, in this work we have demonstrated experimentally, and confirmed theoretically, that phasonic modulation in a quasicrystal can coherently control transport and reversibly tune across a localization-delocalization quantum phase transition. We have shown that these results can be interpreted as manifestations of dynamic localization in the higher-dimensional lattice associated with the quasicrystal, opening up a pathway to simulation of strongly driven quantum Hall systems [41–43]. Combining both phasonic and dipolar driving would allow for complete control of the polarization (linear, elliptical, or circular) of the driving radiation which appears in the superspace, enabling quantum simulation of laser-irradiated integer quantum Hall systems with tunable incident polarization. The interplay between topology and modulation would be a natural direction for further investigation, as the minigap collapse which drives localization also signifies a topological transition [12]. Finally, the sign change of multiple Hamiltonian parameters across Bessel zeros opens up the possibility to design a modulation protocol which reverses the direction of time.

Acknowledgments—We acknowledge support from the Air Force Office of Scientific Research (FA9550-20-1-0240), the NSF QLCI program (OMA-2016245), the NSF Quantum Foundry (DMR-1906325), and the Army Research Office (MURI W911NF1710323). A. E. acknowledges funding by DFG via the Research Unit FOR 2414, under Project No. 277974659. The optical lattices used herein were developed in work supported by the U.S. Department of Energy, Office of Science, National Quantum Information Science Research Centers, Quantum Science Center.

- [1] A. Eckardt, *Rev. Mod. Phys.* **89**, 011004 (2017).
- [2] H. Lignier, C. Sias, D. Ciampini, Y. Singh, A. Zenesini, O. Morsch, and E. Arimondo, *Phys. Rev. Lett.* **99**, 220403 (2007).
- [3] E. Kierig, U. Schnorrberger, A. Schietinger, J. Tomkovic, and M. K. Oberthaler, *Phys. Rev. Lett.* **100**, 190405 (2008).
- [4] D. H. Dunlap and V. M. Kenkre, *Phys. Rev. B* **34**, 3625 (1986).
- [5] M. Holthaus, *Phys. Rev. Lett.* **69**, 351 (1992).
- [6] A. Zenesini, H. Lignier, D. Ciampini, O. Morsch, and E. Arimondo, *Phys. Rev. Lett.* **102**, 100403 (2009).
- [7] S. V. Rajagopal, T. Shimasaki, P. Dotti, M. Račiūnas, R. Senaratne, E. Anisimovas, A. Eckardt, and D. M. Weld, *Phys. Rev. Lett.* **123**, 223201 (2019).
- [8] Y. E. Kraus and O. Zilberberg, *Nat. Phys.* **12**, 624 (2016).
- [9] O. Zilberberg, *Opt. Mater. Express* **11**, 1143 (2021).
- [10] J. Fan and H. Huang, *Front. Phys.* **17**, 13203 (2022).
- [11] P. G. Harper, *Proc. Phys. Soc. London Sect. A* **68**, 874 (1955).
- [12] Y. E. Kraus, Y. Lahini, Z. Ringel, M. Verbin, and O. Zilberberg, *Phys. Rev. Lett.* **109**, 106402 (2012).
- [13] S. Aubry and G. André, *Ann. Isr. Phys. Soc.* **3**, 133 (1980).
- [14] G. Roati, C. D’Errico, L. Fallani, M. Fattori, C. Fort, M. Zaccanti, G. Modugno, M. Modugno, and M. Inguscio, *Nature (London)* **453**, 895 (2008).
- [15] K. Singh, K. Saha, S. A. Parameswaran, and D. M. Weld, *Phys. Rev. A* **92**, 063426 (2015).
- [16] K. Viebahn, M. Sbroscia, E. Carter, J.-C. Yu, and U. Schneider, *Phys. Rev. Lett.* **122**, 110404 (2019).
- [17] M. Sbroscia, K. Viebahn, E. Carter, J.-C. Yu, A. Gaunt, and U. Schneider, *Phys. Rev. Lett.* **125**, 200604 (2020).
- [18] See Supplemental Material at <http://link.aps.org/supplemental/10.1103/PhysRevLett.133.083405> for more details on the experimental setup and theoretical analysis, which includes additional Refs. [19–24].
- [19] S. Ganeshan, J. H. Pixley, and S. Das Sarma, *Phys. Rev. Lett.* **114**, 146601 (2015).
- [20] T. Devakul and D. A. Huse, *Phys. Rev. B* **96**, 214201 (2017).
- [21] A. Eckardt, M. Holthaus, H. Lignier, A. Zenesini, D. Ciampini, O. Morsch, and E. Arimondo, *Phys. Rev. A* **79**, 013611 (2009).
- [22] A. Joushaghani, R. Iyer, J. K. S. Poon, J. S. Aitchison, C. M. de Sterke, J. Wan, and M. M. Dignam, *Phys. Rev. Lett.* **109**, 103901 (2012).
- [23] M. Verbin, O. Zilberberg, Y. Lahini, Y. E. Kraus, and U. Zilberberg, *Phys. Rev. B* **91**, 064201 (2015).
- [24] N. H. Lindner, E. Berg, and M. S. Rudner, *Phys. Rev. X* **7**, 011018 (2017).
- [25] S. Y. Jitomirskaya, *Ann. Math.* **150**, 1159 (1999).
- [26] G. Sun and A. Eckardt, *Phys. Rev. Res.* **2**, 013241 (2020).
- [27] D. R. Hofstadter, *Phys. Rev. B* **14**, 2239 (1976).
- [28] Y. E. Kraus and O. Zilberberg, *Phys. Rev. Lett.* **109**, 116404 (2012).
- [29] M.-C. Chang and Q. Niu, *Phys. Rev. B* **53**, 7010 (1996).
- [30] See the explicit demonstration in Sec. IV of the Supplemental Material [18].
- [31] M. M. Dignam and C. M. de Sterke, *Phys. Rev. Lett.* **88**, 046806 (2002).
- [32] P. Domachuk, C. M. de Sterke, J. Wan, and M. M. Dignam, *Phys. Rev. B* **66**, 165313 (2002).

- [33] F. A. An, K. Padavić, E. J. Meier, S. Hegde, S. Ganeshan, J. H. Pixley, S. Vishveshwara, and B. Gadway, *Phys. Rev. Lett.* **126**, 040603 (2021).
- [34] V. Goblot, A. Štrkalj, N. Pernet, J. L. Lado, C. Dorow, A. Lemaître, L. Le Gratiet, A. Harouri, I. Sagnes, S. Ravets, A. Amo, J. Bloch, and O. Zilberberg, *Nat. Phys.* **16**, 832 (2020).
- [35] K. Rayanov, G. Radons, and S. Flach, *Phys. Rev. E* **88**, 012901 (2013).
- [36] C. Skokos, I. Gkolias, and S. Flach, *Phys. Rev. Lett.* **111**, 064101 (2013).
- [37] O. V. Borovkova, V. E. Lobanov, Y. V. Kartashov, V. A. Vysloukh, and L. Torner, *Phys. Rev. A* **91**, 063825 (2015).
- [38] D. Guzman-Silva, M. Heinrich, T. Biesenthal, Y. V. Kartashov, and A. Szameit, *Opt. Lett.* **45**, 415 (2020).
- [39] A. Eckardt, C. Weiss, and M. Holthaus, *Phys. Rev. Lett.* **95**, 260404 (2005).
- [40] S. Arlinghaus, M. Langemeyer, and M. Holthaus, in *Dynamical Tunneling: Theory and Experiment*, 1st ed., edited by S. Keshavamurthy and P. Schlagheck (CRC Press, Boca Raton, 2011), Chap. 12.
- [41] S. Arlinghaus and M. Holthaus, *Phys. Rev. A* **81**, 063612 (2010).
- [42] M. Wackerl, P. Wenk, and J. Schliemann, *Phys. Rev. B* **100**, 165411 (2019).
- [43] M. Zhao, Q. Chen, X.-D. Tian, and L. Du, *J. Phys. A* **55**, 275003 (2022).